Int. J. Electrochem. Sci., 13 **(2018)** 4020 – 4031, doi: 10.20964/2018.11.39

International Journal of
ELECTROCHEMICAL
SCIENCE
www.electrochemsci.org

Preparation of Hierarchical Porous Carbon Based on Corn-Straw Carbon Nanofiber as an Efficient Electrode Material for Supercapacitors

Gaofeng Shi[*], *Yucan Dong, Guoying Wang , Xia Jiang, Chao Liu, Shiming Jia, Peng zhang, Hua Ma*

School of Petrochemical Engineering, Lanzhou University of Technology,
NO.287, Langongping Road, Lanzhou, Gansu, China
[*]E-mail: shigaofeng@lut.cn

Received: 4 June 2018 / *Accepted:* 30 August 2018 / *Published:* 10 March 2019

Pure PAN and corn-straw carbon mixed nanofibers were prepared by electrospinning. Using a novel method of KOH solid-state activation of nanofibers got hierarchical porous carbon material. The surface area and total pore volume of HPC were 2192.73 $m^2 \cdot g^{-1}$and 1.08 $cm^3 \cdot g^{-1}$, and with an excellent specific capacitance of 376.5 $F \cdot g^{-1}$ at a current density of 0.5 $A \cdot g^{-1}$, remaining a capacitance retention of 94.18% after 5000 cycles at the current density of 2$A \cdot g^{-1}$. This new material has excellent electrochemical performance and can be used as an electrode material for supercapacitors.

Keywords: Electrospinning method; hierarchical porous carbon; electrode materials; capacitive performance

1. INTRODUCTION

As global demand for energy has grown, researchers have been intrigued by the widespread interest in energy storage and energy transfer exploration. Compared with conventional capacitors and batteries, supercapacitors are one of the innovations in the field of electrical energy storage device with high power density, high discharge capacity, excellent circulation performance and low cost of use[1-3]. As a result, supercapacitors have been widely used in fields such as wearable electronics， electric vehicle, renewable energy grids, backup power supplies, and aerospace [4-7] .

High-surface-area carbon is the material of choice, as it combines a large surface area wetted by the electrolyte, high electronic conductivity, and chemical and electrochemical stabilities with low cost [1]. Based on the basic mechanism, supercapacitors have various carbons materials, such as activated

carbons, graphene, carbon nanotubes and activated carbon nanofibers [8-14]. Among the carbon materials, the graphene is widely used in the supercapacitors with its excellent conductivity, thermal conductivity and high mechanical strength, large specific surface area, but the traditional preparation methods of graphene have certain defects, which can't achieve the industrialization production of graphene [10, 15]. So researchers have tried to find other materials to replace graphene.

For green development concept, to reduce the consumption of fossil fuels, many researchers have been increasingly utilized the biomass by-products from the forestry and corps residues such as fungi, argan seed shells, wheat-straw, spinach-leaves, sunflower seed shell as super capacitor grade carbon materials particularly in some agricultural countries [16-20]. China, a big agricultural country, has a vast potential for future development in the biomass by-products.

Compared with other biological materials, corn stalks are rich in source and easy to handle. In this paper, we have obtained the porous carbon nanomaterials by electrospinning and peroxidation, carbonization. The morphology, pore structure and specific area of the porous carbon nanofibers were investigated by FE-SEM, FT-IR, XRD, and BET methods. Finally, we investigated the electrochemical performance of the porous carbon nanofibers with the way of cyclic voltammetry (CV), galvanostatic discharge (GCD) and electrochemical impedance spectroscopy(EIS). In this way, we explored the application of porous carbon nanomaterials made from corn-straw to supercapacitor electrode materials.

2. EXPERIMENTAL

2.1 Instruments and reagents

2.1.1 Instruments

The electrospinning apparatus (Yongkang Leye Science and Technology Development Co., Ltd., China.); TL1200 tube furnace (Hefei Ke Jing Materials Technology Co., Ltd., China); Infrared spectroscopy was performed using a Fourier transform infrared spectrometer (Nicolet, USA); D/max-2400 X-ray diffractometer (Rigaku Corporation , Japan) ;JSM-6701F cold field emission scanning electron microscope(JOEL Japan); CHI660E Electrochemical workstation (Shanghai Chenhua Instrument Co., Ltd., China).

2.1.2 Reagents

Corn stalks, got it in Gansu, China 2017; Polyacrylonitrile(PAN, Mw=150,000), nikel foam were obtained from Macklin, Shanghai, China; N,N-dimethylformamide， hydrogen peroxide were purchased from Tianxin Fine Chemical Development Center, China; purchased acetylene black from Tianjin UNITA excellent Chemical Technology Co., Ltd., Tianjin, China; acquired potassium hydroxide and concentrated sulfuric acid from BASF, Tianjin, China; purchased teflon from Guangzhou Songbai Chemical Industry Co., Ltd., Guangzhou, China.

2.2. Experimental method

2.2.1 Pretreatment of corn-straw

Take a certain amount of corn-straw, crush and wash with benzene, ethanol, and distilled water for three times and then dry at 80°C for 24 hours. Weigh accurately dried corn-straw 20.003g into a 500mL beaker, after that, add concentrated sulfuric acid 150ml slowly and stir continuously for 30 minutes. Then slowly add H_2O_2 50ml while stirring for about 90 minutes. Wash with distilled water several times close to neutral under room temperature, and then, the mixture is centrifugally separated at 2000 r/min. Obtain the corn-straw carbon sample after dry the filter cake at 80℃ for 48h.

2.2.2 Preparation of corn-straw carbon-based nanofibers

We added polyacrylonitrile(PAN, Mw=150,000) 1.6g and biomass carbon 0.4g into N,N-dimethylformamide(DMF) 20mL and then stirred for 6h at 25°C. Then ultrasonically disperse for 2 hours after complete dissolution fully to thoroughly mix polyacrylonitrile(PAN) and corn-straw. The PAN/corn-straw solution was placed in a syringe and ejected under 18 kV between the syringe needle and a rotating collector at a distance of 20 cm to form nanofibers [2]. Pure PAN-based nanofibers were prepared using the same method.

2.2.3 Preparation of hierarchical porous carbon

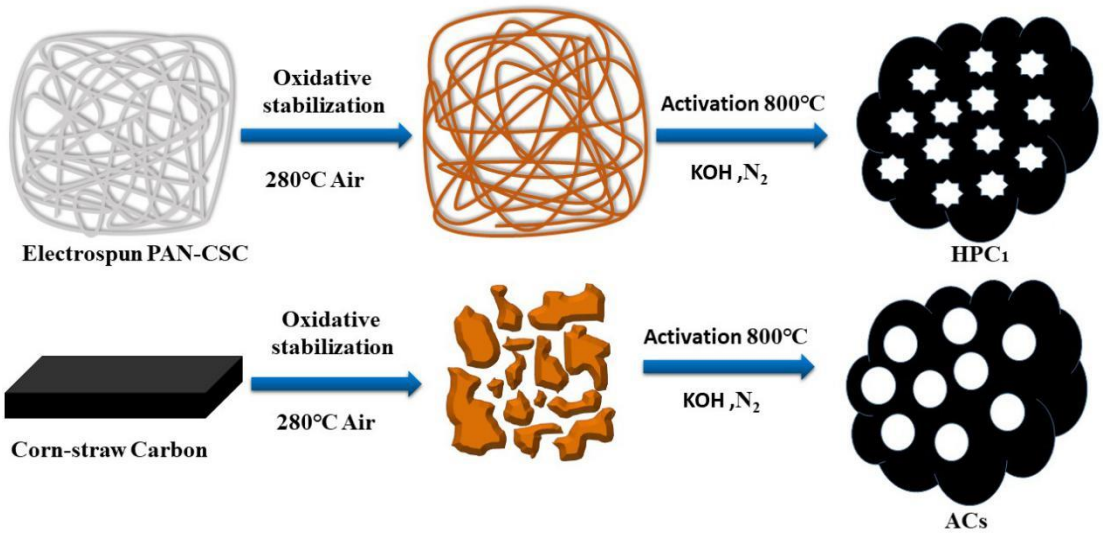

Figure 1. Scheme for the processing of HPC_1, ACs.

Put nanofibers into the muffle furnace and rise the temperature up to 260 ^{0}C at 1^{0}C·min^{-1} heating rate for pre-oxidation 2 hours in air atmosphere [21]. Solid KOH was added to the stabilized nanofibers at a 1:2 w/w ratio (nanofibers/KOH) and ground in an agate mortar for 20 minutes. Then, the mixture was placed in a tube furnace under nitrogen atmosphere. The tube furnace was raised to 700 ^{0}C at a heating rate of 2 ^{0}C/min and held for two hours. The activated and carbonized products were washed

with 6mol/L HCl solution two times, and then, washed with distilled water several times until the pH of the filtrate is about 7. The final products were dried in an oven at 80^0C for 24 h, and the hierarchically porous carbon were obtained. Activated carbon (ACs) was prepared by the same steps as described above and was named ACs, except for the electrospinning step. Hierarchical porous carbon from pure PAN carbon nanofibers and PAN-C nanofibers were noted HPC_0 and HPC_1, respectively. The prepared samples are listed in Fig. 1.

3. RESULT AND DISCUSSION

3.1 Surface morphologies of the samples

From Fig. 2(A)(B), it can be seen that pure PAN and PAN-C nanofibers were obtained by electrospinning. The average diameter of the pure PAN nanofibers is 240.6 nm, while the diameter of the nanofibers of PAN-C decrease to 180.2 nm. This is because the addition of carbon increases the conductivity of the precursor solution and is stretched by the higher electric field force in the high voltage electrostatic field [22]. Fig. 2(C)(D)(E) shows a large number of irregular pore structures appear in HPC_1、HPC_0、and ACs due to chemical activation of KOH. Interestingly, a large number of small pore structures appear in the HPC_1 macrospore wall as shown in Fig. 2(C'). The above results indicate that carbon nanomaterials with different pore shapes are well prepared by carbon nanofibers.

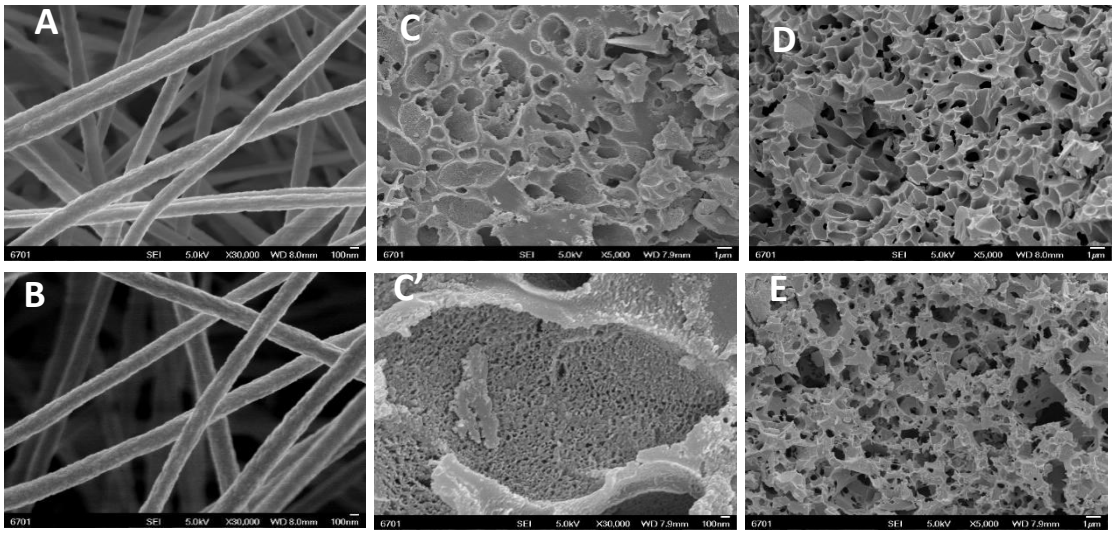

Figure 2. SEM images of PAN(A) and PAN-C nanofibers(B) before carbonization, HPC_1(C), (C'), HPC_0(D), and ACs(E).

3.2 Infrared spectra of nanofibers and hierarchical porous carbon

As shown the Fig. 3, the absorption peaks of PAN nanofibers and PAN-C nanofibers are relatively weak, indicating that there are less functional groups on the surface. The characteristic peaks at 1228 cm^{-1}, 1587 cm^{-1}, and 3409 cm^{-1} of HPC_0 and HPC_1 which prepared after carbonization and

activation with KOH solid-state are significantly enhanced, which are assigned to the stretching vibrations of -C-O, -C=C, and -OH on the surface of the samples respectively[16]. The enhanced peaks at 2854 cm^{-1} and 2923 cm^{-1} are due to the antisymmetric and symmetric stretching vibrations of -C-H. These enhanced peaks suggest that the oxygen-containing groups on the surface of the material are significantly increased, thereby increasing the wettability of the electrolyte and facilitating the improvement of the electrochemical performance of the material.

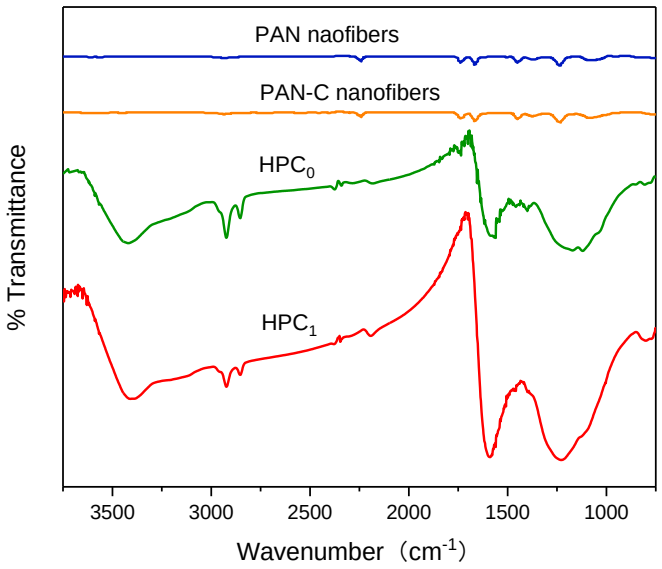

Figure 3. Infrared spectra of PAN and PAN-C nanofibers, HPC_1, HPC_0.

3.3 X-ray diffraction of hierarchical porous carbon and ACs

To further examine the structures of the samples, XRD characterization was performed. The results are shown in Fig. 4. The broad peak at around 2θ=23°for the diffraction pattern of all samples is due to the parallel-laminated graphene layers (PLGLs) reflection from the (002) crystal planes, while the weak peak at around 2θ=42°was attributed to the (101) crystal planes of SP^2-C [23]. The diffraction curves are broad and blunt peaks, indicating that the sample is a turbostratic carbon structure [24]. The KOH solid activation destroys the fiber structure, increases the disorder of the sample structure, and leads to the destruction of the graphite layer. The peak of ACs at about 2θ=23° is sharper than that of HPC_1 and HPC_0, because during the electrospinning process, the polymer chains are rapidly stretched and cured by the high-voltage electrostatic field force, and there is not enough time to form a 3D ordered crystal structure[25]. Activation more likely attacks defect site, and further increase the degree of carbon disorder.

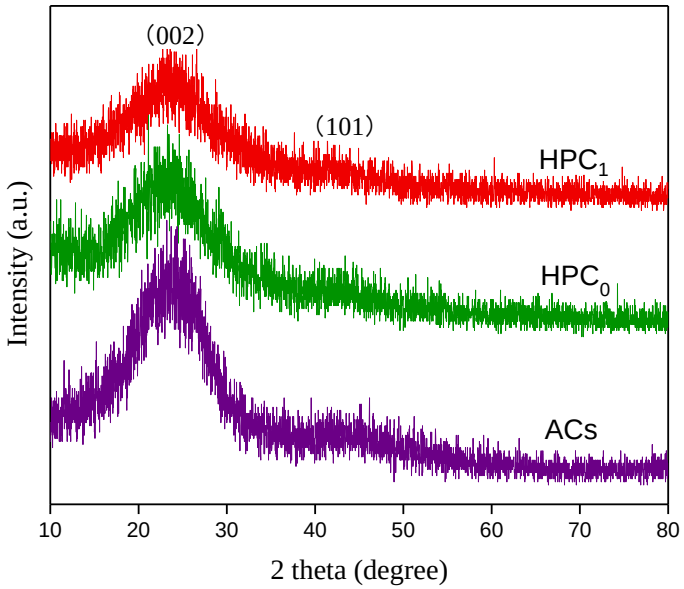

Figure 4. X-ray diffraction of HPC_1, HPC_0, and ACs

3.4 N_2 adsorption/ desorption isotherms of HPC and ACs.

As shown in Fig. 5, the isothermal adsorption curve of HPC_1 belongs to I (a) type, suggesting that the material is mainly composed of microporous structure[26]. The N_2 absorption of the material at P/P_0 ~ 0.4 to 0.6 is indicative of the generation of mesopores. Indeed, the pore size distribution curve also proves that the material has mesopores with a diameter of about 11 nm. The sharp capillary condensation step at high relative pressure implies that HPC_1 has a certain number of large pore structures[27].Table 1 shows the surface area and total pore volume of HPC_1 were 2192.73 $m^2 \cdot g^{-1}$and 1.08 $cm^3 \cdot g^{-1}$, while that of HPC_0 was only 971.87 $m^2 \cdot g^{-1}$ and 0.43 $cm^3 \cdot g^{-1}$. The reason is that during KOH solid high temperature activation was over 400°C, K_2CO_3 was generated, and reacted with carbon to form a pore framework, subsequently. Further, the gaseous H_2, H_2O, CO or CO_2, which were generated from the reaction, attacked the pores, and caused the fibers to collapse [15]. And the addition of corn-straw carbon increases the modulus of the stabilized composite nanofibers, improves the mechanical properties, and the collapse was less than that of pure PAN nanofibers, forming more large pores [28]. The reactive gas erodes the inner walls of mac/mesopores at high temperatures, forming a large number of micropores. This is consistent with the SEM image. The micropores are located in the inner walls of the mac/mesopores, the diffusion distance from the mesopores to the mac/micropores is very short, and the infrared spectra shows a large number of oxygen-containing groups on the surface. This structure provides a fast channel for electron transfer in the electrolyte. These characters enable HPC_1 to exhibit high capacitance and cycle durability in supercapacitors[29]. The surface area of ACs is lower than that of HPC which is mainly because the area of nanofibers contact activator during activation is much larger than that of bulk corn-straw carbon.

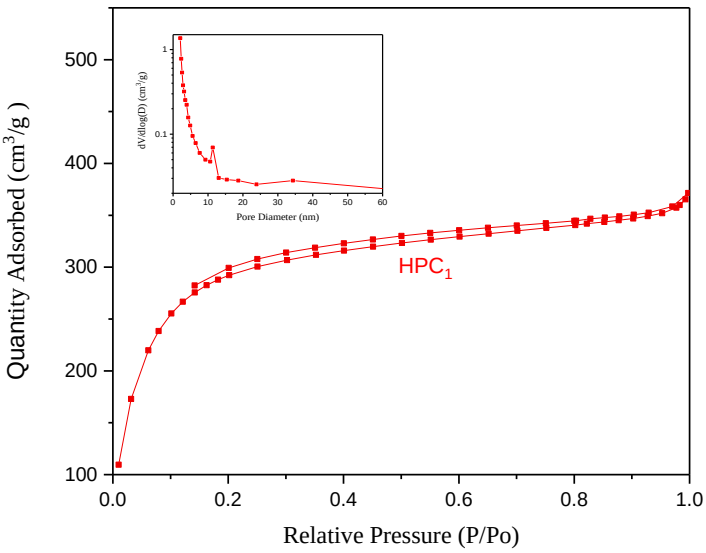

Figure 5. Nitrogen adsorption isotherms and the pore size distribution of HPC_1

Table 1. BET surface area and porosity characteristics of the HPC and ACs

Sample name	S_{BET}(m^2 g^{-1})	$S_{micropore}$ (m^2 g^{-1})	$V_{total\ pore}$ (cm^3 g^{-1})	$V_{micropore}$(cm^3 g^{-1})
HPC_1	2192.73	1391.96	1.08	0.63
HPC_0	971.87	743.32	0.43	0.34
AC_S	596.66	475.53	0.31	0.22

3.5 Electrochemical properties of the HPC and Acs

The cyclic voltammetry and galvanostatic charge and discharge measurements were performed in a three-electrode system with 6M KOH aqueous solution as the electrolyte, a Pt electrode as the counter electrode, and a saturated calomel electrode as the reference electrode. Pressing a mixture of 95wt% and 5wt% polytetrafluoroethylene (PTFE) binder into foamed nickel at a pressure of 350 kg/cm ^{2} and then dried at 80°C under vacuum prepared the electrode samples.

As Fig. 6(A)(B) shows, the CV curves of the samples are all rectangular-like shape and have weak redox peaks, and the galvanostatic charge-discharge curve is an isosceles triangle shape and the linear deviation is small, which means that porous carbon materials with oxygen-containing groups possess good capacitive behaviors which is originated from the combination of electric double layer capacitance and pseudocapacitance[29]. The specific capacitance (Cm) of the electrode is estimated from the charge-discharge curve by using the following equation [30-31].

$$C = \frac{I\Delta t}{m\Delta V} \quad (1)$$

Where I and Δt are respectively discharge current and discharge time, m is the mass of the active materials, ΔV is the voltage range. The specific capacitances of HPC_1, HPC_0, and ACs electrodes were respectively 332.3F·g^{-1}, 184.3F·g^{-1} and 238.7F·g^{-1} at the current density of 1 A·g^{-1}. It is clear that the capacitance performance of HPC_1 electrode is the best, which is consistent with the CV curves, due to

the effective surface area of HPC_1 is much larger than that of HPC_0 and ACs. ACs have better capacitance performance than HPC_0 because there are more disordered carbon and defective graphite structures in the HPC_0 material as XRD curves shows even though the effective surface area of HPC_0 is slightly larger than ACs. The performance of these samples is dominated by the conductivity property [24,27]. Fig. 6C shows as the scanning speed increases from 5 $mV \cdot s^{-1}$ to 100 $mV \cdot s^{-1}$, the degree of deviation from the rectangular curve becomes large. This is because the voltage changes to speed up as the scan rate increased, the current response increased, the electrolyte can not fully diffuse into the electrode. In other words, there is no time for the electrolyte to fully enter the small aperture, the effective specific surface area is reduced, the resistance of the capacitor increased, resulting in poor performance of the capacitor [32]. Even at current densities up to 10 $A \cdot g^{-1}$, all curves show a close to an isosceles triangle shape, revealing a close to ideal capacitive behavior (Fig. 6D). It can be seen that when the current densities decrease from 0.5$A \cdot g^{-1}$ to 10$A \cdot g^{-1}$, the specific capacitance of HPC_1 decrease from 375.6 $F \cdot g^{-1}$ to 270$F \cdot g^{-1}$ with 71.88% for capacitance retention rate (Fig.6E). For a better comparison, the performance of this working hierarchically porous carbon electrode material and other electrode materials is summarized in Table 2. According to Fig. 6G, the specific capacitance retention is 96.4% after galvanostatic charge-discharge 5000 cycles at a current density of 2 $A \cdot g^{-1}$, showing an excellent cyclic stability. The above analysis proves that the excellent capacitance performance of HPC_1 can be used as a supercapacitor electrode material.

Table 2. Comparison of electrochemical performance of hierarchically porous carbon with other different materials

Electrode materials	Specific capacitance(current density)	Electrolyte	S_{BET} ($m^2 g^{-1}$)	Referencces
Hierarchically porous carbon based on banana peel	206 $F \cdot g^{-1}$ (1A g^{-1})	6 mol L^{-1} KOH	1650 $m^2 g^{-1}$	[34]
Hierarchically porous and heteroatom doped carbon derived from tobacco rods	286.6 $F \cdot g^{-1}$ (0.5 A g^{-1})	6 mol L^{-1} KOH	2115 $m^2 g^{-1}$	[35]
Hierarchically porous N-Doped carbon nanosheets derived from grapefruit peels	311 $F \cdot g^{-1}$ (0.1 A g^{-1})	1 mol L^{-1} Na_2SO_4	1760 $m^2 g^{-1}$	[36]
Hierarchically porous carbon derived from cotton fabric	360 $F \cdot g^{-1}$ (0.5 A g^{-1})	6 mol L^{-1} KOH	777 $m^2 g^{-1}$	[37]
Hierarchically porous carbon derived from biomass	160.5 $F \cdot g^{-1}$ (0.2 A g^{-1})	EC and DEC(1:1)	1994 $m^2 g^{-1}$	[38]
Hierarchical porous carbon based on corn-straw carbon nanofiber	376.5 $F \cdot g^{-1}$(0.5 A g^{-1})	6 mol L^{-1} KOH	2192.73 $m^2 \cdot g^{-1}$	This work

Fig. 6G shows the electrochemical impedance spectra (EIS) of the materials and the fitting of equivalent circuit model. In the high frequency region, the point intersecting the real axis reflects the internal resistance (Rs) of the electrode material, and the semicircle corresponds to the charge transfer resistance (Rct). The nearly vertical line in the low frequency region represents the diffusion resistance (W) of the electrolyte in the porous structure [33]. The reason for the lower slope of the ACs in the low-frequency region of the HPC is that the disordered carbon and defective graphite structure affect the conductivity.

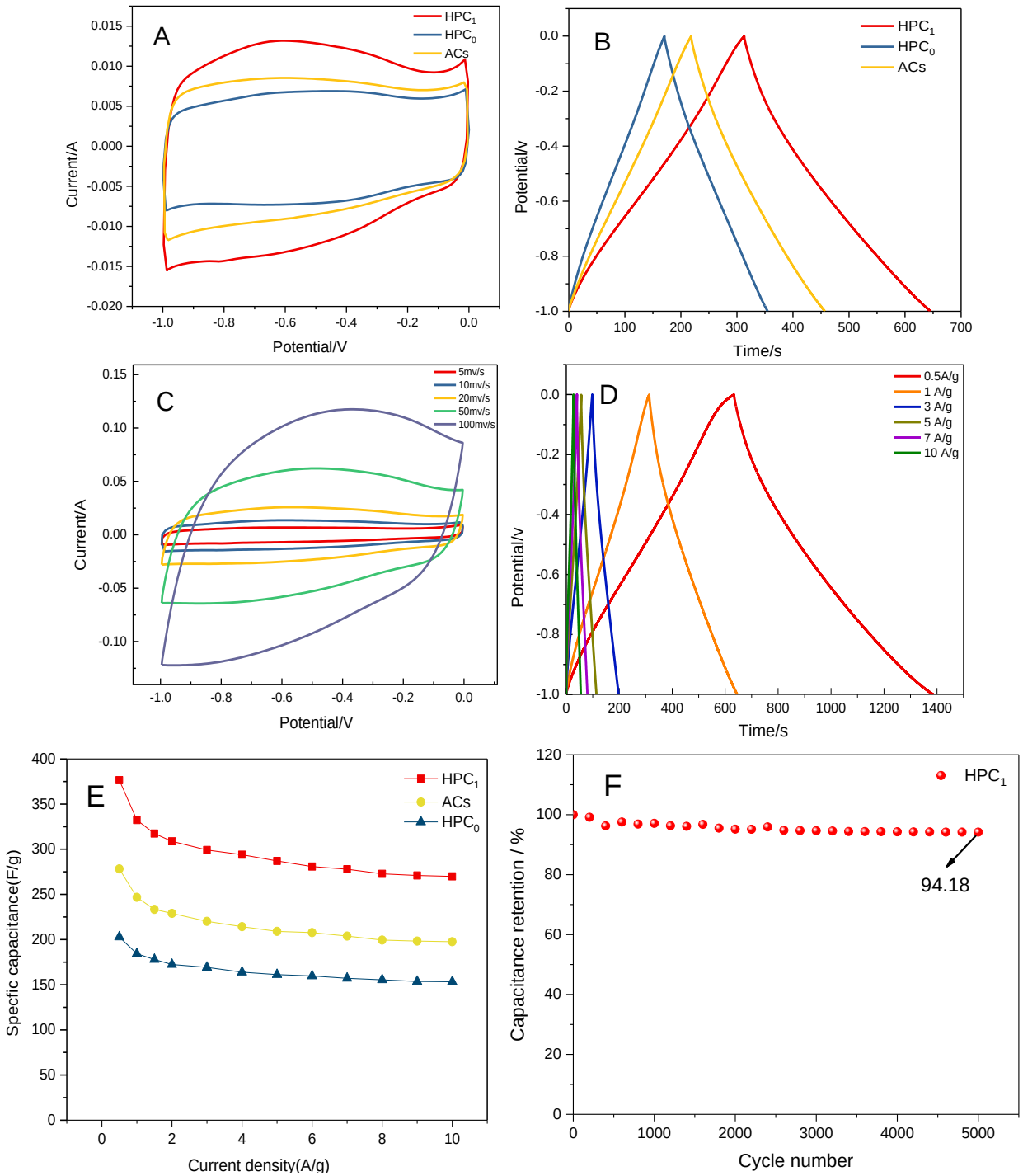

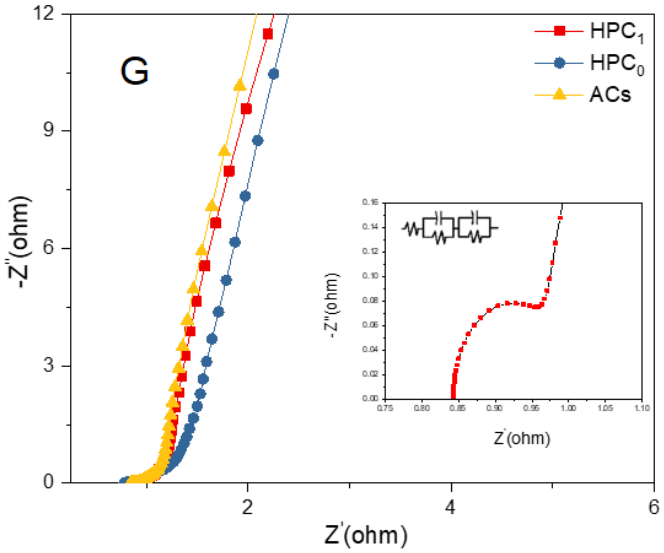

Figure 6. Electrochemical performance of HPC and ACs electrode in three electrode system. CV curves at 20mV sweep rate(A) and charge-discharge curves at a current density of 1A·g^{-1}(B) of HPC_1, HPC_0 and ACs. (C) and (D) shows CV at different scan rate and charge-discharge curves at different current density of HPC_1; Specific capacitance changes of HPC_1, HPC_0 and ACs electrodes at different current densities(E); Specific capacitance retention rates at the current density of 2 A·g^{-1} after 5000 cycles(F). Electrochemical impedance spectra (EIS) of HPC_1, HPC_0 and ACs(G).

The slope of HPC_1 is higher than that of HPC_0 in the low frequency region, indicating that adding corn-straw carbon increases the charge transfer energy and improves the electrochemical performance of the electrode.

4. CONCLUSIONS

In summary, the HPCs active electrode material prepared by KOH solid-state activation of corn-straw carbon mixed nanofiber (2:1 w/w ratio) has a special pore structure. This electrode material has good capacitance performance with a specific capacitance of 376.5 F·g^{-1} at a current density of 0.5 A·g^{-1}. The capacitance retention rate was 94.18% after 5000 cycles at a current density of 2 A·g^{-1}, indicating that the material has good cycle stability. This study not only improves the utilization efficiency of biomass resources, but also prepares high-performance electrode materials that can be used for supercapacitors.

ACKNOWLEDGEMENTS
This work was supported by the National Natural Science Foundation of China (21567015), and the National Key Research and Development Program of China(2016YFC0202900).

References

1. M. Winter and R. J. Brodd, *J. Cheminform.*, 104(2004)4245.
2. H. Y. Lee and J. B. Goodenough, *J. Solid State Chem.*, 144(2015)220-223.
3. S. Wang, N. Liu, J. Su, L. Li, F. Long, Z. Zou, X. Jiang and Y. Gao, *Acs. Nano.*, 11(2017)2066.

4. K. Jost, D. Stenger, C. R. Perez, J. K. McDonough, K. Lian, Y. Gogotsi and G. Dion, *Energy & Environ. Sci.*, 6(2013)2698-2705.
5. Y. Yang, Q. Huang, L. Niu, D. Wang, C. Yan, Y. She and Z. Zheng, *Adv. Mater*., 29(2017)1606679.
6. Z. Song, H. Hofmann, J. Li, X. Han, X. Zhang, M. Ouyang, *J. Power Sources*, 274 (2015)400-411.
7. L. Yao, Q. Wu, P. Zhang, J. Zhang, D. Wang, Y. Li, X. Ren, H. Mi, L. Deng and Z. Zheng, *Adv. Mater*., (2018)1706054.
8. F. Miao, C. Shao, X. Li, K. Wang and Y. Liu, *J. Mater. Chem*., A,4(2016)4180-4187.
9. J. Yu, W. Lu, S. Pei, K. Gong, L. Wang, L. Meng, Y. Huang, J. P. Smith, K. S. Booksh, Q. Li, J. H. Byun, Y. Oh, Y. Yan and T. W. Chou, *Acs. Nano*.,10(2016)5204-5211.
10. S. Zheng, Z. Wu, S. Wang, H. Xiao, F. Zhou, C. Sun, X. Bao and H. Cheng, *Energy Storage Mater*., 6(2017)70-97.
11. A. Ameli, M. Nofar, C. B. Park, P. Potschke and G. Rizvi, *Carbon*, 71(2014)206-217.
12. M. Zhi, S. Liu, Z. Hong and N. Wu, *Rsc. Adv*., 4(2014)43619-43623.
13. K. Wang, Y. Cao, X. Wang, Q. Fan, W. Gibbons, T. Johnson, B. Luo and Z. Gu, *Energy*, 94(2016)666-671.
14. L.L. Zhang, R. Zhou, and X.S. Zhao, *J. Mater.Chem*, 20(2010)5983-5992.
15. Y.W. Zhu, S. Murali and M. D. Stoller, *Sci*., 332(2011)1537-1541.
16. W. Yang, Z.R. Shi, H. Guo, J. Guo, X. Lei and L.G. Yue,. *Int. J. Electrochem Sci*., 12(2017)5587-5597.
17. C. Liu, G. Han, Y. Chang, Y. Xiao, M. Li, W. Zhou, D. Fu and W. Hou, Ch*emelectrochem*, 3(2016)323-331.
18. Y. Ou, C. Peng, J. Lang, D. Zhu and X. Yan, *New Carbon Mater*., 77(2014)1196-1196.
19. X. Li, W. Xing, S. Zhuo, J. Zhou, F. Li, S. Qiao and G. Lu, *Bioresour. Technol*., 102(2011) 1118-1123.
20. Y. Lv, L. Gana, M. Liu, W. Xiong, Z. Xu, D. Zhu and D. S. Wright, *J. Power Sources*, 209(2012)152-157.
21. Y. S. Yun, C. Im, H. H. Park, I. Hwang, Y. Tak and H. J. Jin, *J. Power Sources*, 234(2013)285-291.
22. S. Prilutsky, E. Zussman and Y. Cohen, *Nanotechnol.*, 19(2008)165603.
23. D. Qin and S. A. Chen, *J. Solid State Electrochem*., 21(2017)1305-1312.
24. L. Zhang, Y. Jiang, L. Wang, C. Zhang and S. Liu, *Electrochimica Acta*, 196(2016)189-196.
25. R. Jalili, M. Morshed and S. A. H. R, *Applied Polymer Sci*., 101(2010)4350-4357.
26. M. East, *Pure Applied Chem*., 38(2016)25-25.
27. H. Feng, M. T. Zheng, H. Dong, Y. Xiao, H. Hu, Z. Sun, C. Long, Y. Cai, X. Zhao, H. Zhang, B. Lei and Y. Liu, *J. Mater. Chem*. A, 3(2015)15225-15234.
28. F. Ko, Y. Gogotsi, A. Ali, N. Naguib, H. Ye, G. Yang, C. Li and P. Willis, *Adv. Mater*, 15(2003)1161-1165.
29. G. Wang, J. Zhang, S. Kuang, J. Zhou, W. Xing and S. Zhuo, *Electrochim. Acta*, 153(2015)273-279.
30. L. Chen, X. Zhang, H. Liang, M. Kong, Q. Guan, P. Chen, Z. Wu and S. Yu, *Acs. Nano*., 6(2012)7092-7102.
31. S. Chen, J. Zhu, X. Wu, Q. Han and X. Wang, *Acs. Nano*., 4(2010)2822.
32. H. Feng, M. T. Zheng, H. Dong, Y. Xiao, H. Hu, Z. Sun, C. Long, Y. Cai, X. Zhao, H. Zhang, B. Lei and Y. Liu, *J. Mater. Chem*. A, 3(2015)15225-15234.
33. B. C. Kima , H. T. Jeongb , C. J. Raja , Y. R. Kimb , B. B. Choa , K. H. Yu and S. Met., *Synth Met*,207(2015)116-121.
34. Y. Lv, L. Gan, M. Liu, W. Xiong, Z. Xu, D. Zhu and D. S. Wright, *J. Power Sources*, 209(2012)152-157.
35. Y. Zhao, M. Lu, P. Tao, Y. Zhang, X. Gong, Z. Yang, G. Zhang and H. L, J. *Power Sources*,

307(2016)391-400.
36. Y. Wang , B. Hou, H. Lü, C. Lü and X. Wu, C*hemistryselect*, 1(2016)1441-1447.
37. L. Chen, T. Ji, L. Mu and J. Zhu, *Carbon*, 111(2017)839-848.
38. J. Chen, X. Zhou, C. Mei, J. Xu, S. Zhou and C. Wong, *J. Power Sources*, 342(2017)48-55.